ANTIOXIDANTS & REDOX SIGNALING
Volume 31, Number 18, 2019

DOI: 10.1089/ars.2018.7614

Discoveries

ORIGINAL RESEARCH COMMUNICATION

Impaired Peroxisomal Fitness in Obese Mice, a Vicious Cycle Exacerbating Adipocyte Dysfunction *via* Oxidative Stress

Lingjuan Piao,[1,2,*] Debra Dorotea,[1,*] Songling Jiang,[1] Eun Hee Koh,[2,3] Goo Taeg Oh,[4] and Hunjoo Ha[1]

Abstract

Aims: Peroxisome is a critical organelle for fatty acid oxidation (FAO) and metabolism of reactive oxygen species (ROS). Increased oxidative stress in adipose tissue contributes to the development of insulin resistance and metabolic syndrome in obesity. This study aimed to investigate the role of peroxisomal fitness in maintaining adipocyte function, which has been under-rated in the obesity research area.
Results: Reduced peroxisomal gene expressions in white adipose tissue (WAT) of obese mice suggested a close correlation between peroxisomes and obesity. Peroxisomal biogenesis factor 5 siRNA increased cellular ROS and inflammatory mediators in 3T3-L1 adipocytes. On the contrary, hydrogen peroxide or tumor necrosis factor-α treatment significantly decreased biogenesis- and function-related peroxisomal proteins, suggesting a positive feedback loop of ROS/inflammation and peroxisomal dysfunction. Correspondingly, catalase (a major peroxisomal antioxidant)-knockout mice fed with high-fat diet (HFD) exhibited suppressed peroxisomal proteins along with increased oxidative stress and accelerated obesity. In response to fenofibrate (a peroxisomal proliferator) treatment, WAT of HFD-fed wild-type mice showed not only increases in peroxisomal biogenesis and FAO but also attenuated features of adipocyte dysfunction and obesity. However, these results were not observed in peroxisome proliferator-activated receptor-alpha null obese mice.
Innovation: Impaired peroxisomal fitness enhanced oxidative stress and inflammation in adipocytes, which exacerbates obesity.
Conclusion: Adipose tissue peroxisomal homeostasis plays an important role in attenuating the features of obesity, and it can be a potential therapeutic target of obesity. *Antioxid. Redox Signal.* 31, 1339–1351.

Keywords: obesity, peroxisome, white adipose tissue, catalase, PPARα, fenofibrate

Introduction

THE PREVALENCE OF OBESITY has been steadily increased, and obesity has become one of the most serious worldwide health problems (24). Accumulating evidence has indicated that obesity is related to various diseases, such as dyslipidemia, insulin resistance, and type 2 diabetes (37). Obesity is defined as an excessive fat accumulation in the adipose tissue, which is a result of energy imbalance between energy intake and expenditure. Adipose tissues represent ~10% of body weight in lean adults, but it can achieve up to 50% in obese subjects (15). Hypertrophic adipose tissue with increased oxidative stress exhibited disturbed redox balance, which consequently leads to impaired adipogenesis, insulin resistance, and obesity (7). However, the underlying mechanism of oxidative stress in adipose tissue remains elusive.

Peroxisomes are small, membrane-enclosed organelles that are present in all cell types, except for erythrocytes. These organelles play a critical role in metabolism of reactive oxygen species (ROS) and various lipids, such as very long-chain fatty acid (VLCFA) β-oxidation, branched-chain fatty acid α-oxidation, and ether phospholipid biosynthesis

[1]Graduate School of Pharmaceutical Sciences, College of Pharmacy, Ewha Womans University, Seoul, Republic of Korea.
[2]Asan Institute for Life Sciences, University of Ulsan College of Medicine, Seoul, Republic of Korea.
[3]Department of Internal Medicine, University of Ulsan College of Medicine, Seoul, Republic of Korea.
[4]Department of Life Sciences, Ewha Womans University, Seoul, Republic of Korea.
*These two authors contributed equally to this work.

Innovation

Peroxisome defects have been associated with adipocyte dysfunction. However, the role of peroxisome in adipocyte redox homeostasis remains elusive. We showed decreases in a set of peroxisomal genes in white adipose tissue of mice and human with obesity. Impaired peroxisomal fitness significantly enhanced oxidative stress and inflammation in adipocytes, which eventually aggravates obesity. Fenofibrate (peroxisome proliferator-activated receptor agonist) treatment in high-fat diet-induced obese mice increased peroxisomal biogenesis-related proteins, restored peroxisomal fatty acid oxidation, and attenuated the features of adipocyte dysfunction and obesity. Thus, adipose tissue peroxisome can be a new therapeutic target in obesity-associated metabolic syndrome.

(29). Enhanced cellular oxidative stress by peroxisome defects or dysfunction has been implicated with aging, type 2 diabetes, and neurodegenerative disorders (4, 10, 12). Growing evidence has suggested the relation between peroxisomes and adipose tissue function. Increased peroxisome numbers were observed during adipogenesis of 3T3-L1 adipocytes (31).

Peroxisomes are dynamic organelles that rapidly assemble, multiply, and degrade in response to metabolic need. For their biogenesis, they require a group of proteins called peroxins. Peroxisomal biogenesis factor 16 (Pex16) promotes peroxisomal growth *via* Pex3-dependent integration of peroxisomal membrane proteins. Pex16-silencing adipocytes exhibited decreased adipogenesis and adipocyte lipid metabolism due to deficient peroxisome number (19). Whereas Pex5 is the import receptor of peroxisomal matrix proteins for formatting functional peroxisome. Adipose tissue-specific Pex5 knockout (KO) mice exhibited dysfunctional peroxisomes in adipose tissue with reduced lipolysis, increased fat mass, and insulin resistance (30). In contrast, a peroxisomal proliferator-activated receptor alpha (PPARα) agonist treatment ameliorated adiposity and insulin resistance in obese mice (23). Nevertheless, the role of peroxisome in redox homeostasis of adipose tissue has not been clearly elucidated.

In this study, we aimed to dissect the role of peroxisome in redox homeostasis of adipose tissues under high-fat diet (HFD)-induced metabolic disorders. We initially demonstrated decreases in peroxisomal biogenesis in both genetic- and diet-induced obese mice. Hydrogen peroxide (H_2O_2) and tumor necrosis factor-α (TNF-α) decreased peroxisomal biogenesis, and loss of Pex5 function, in turn, exacerbated inflammation and oxidative stress in 3T3-L1 adipocytes. We confirmed that peroxisomal oxidative stress led to decreased peroxisomal biogenesis and enhanced inflammation in white adipose tissue (WAT) of HFD-fed catalase KO (CKO) mice. Then, we investigated whether fenofibrate, a peroxisomal proliferator, might rescue peroxisomal biogenesis and function in HFD-induced adipocytes dysfunction.

Results

Peroxisomal abundance is decreased in WAT of obese mice

Our preliminary result demonstrated increased peroxisomal genes during adipogenesis of 3T3-L1 adipocyte (Supplementary Fig. S1A–G). We initially, therefore, investigated whether peroxisome abundance was altered in db/db mice, which exhibit insulin resistance and obesity (Supplementary Fig. S2). We examined a set of peroxisomal genes involved in peroxisomal biogenesis, including import receptor (Pex5 and Pex7), docking complex (Pex13 and Pex14), membrane assembly (Pex16 and Pex19), and elongation (Pex11α) (14). Almost all of these genes were significantly lower in db/db mice than in db/m^+ mice (Fig. 1A).

As peroxisomes are functionally required for fatty acid oxidation (FAO) and ROS detoxification, we measured mRNA expression of ATP-binding cassette subfamily D member 2 (Abcd2), Abcd3, acyl-CoA oxidase 1 (Acox1), acetyl-CoA acyltransferase 1A, acyl-CoA thioesterase 4 (Acot4), as well as catalase. These functional genes were significantly decreased in db/db mice compared with db/m^+ mice (Fig. 1A). A lower immunostaining intensity of Abcd3, a marker of peroxisomal membrane protein, was observed in db/db mice in comparison with db/m^+ mice, further confirming decreased peroxisomal abundance in WAT (Fig. 1B). The reductions of peroxisomal biogenesis genes and peroxisome abundance in adipose tissue were also found in HFD-fed mice as compared with normal diet (ND)-fed mice (Fig. 1C, D).

Altogether, peroxisomal biogenesis and abundance are downregulated in WAT of both diet- and genetically induced obese mice, suggesting a role of WAT peroxisome in the development and progression of obesity.

Pex5 knockdown leads to increased oxidative stress and inflammation in 3T3-L1 adipocytes

Altered peroxisomal genes may be either a causal or a collateral effect of hypertrophic adipocytes. We elucidated this key event by analyzing pathological changes initiated by loss of peroxisomal function.

Knockdown of Pex5, a crucial peroxin involved in peroxisome biogenesis, in 3T3-L1 adipocytes led to downregulation of Pex11α, Pex14, Pex16, Pex19, Acox1, and catalase mRNA levels (Fig. 2A), and Pex5, Abcd3, and catalase protein expression (Fig. 2B, C). Loss of Pex5 function in adipocytes led to decreases in peroxisome abundance (Fig. 2D, E), total peroxisomal FAO (Fig. 2F), and C26:0 FAO (Fig. 2G). 2′,7′–dichlorofluorescein diacetate (DCF-DA) staining further revealed higher cytosolic ROS in Pex5 knockdown adipocytes than those in control adipocytes (Fig. 2H, I). Interestingly, transcript levels of inflammatory mediators, that is, TNF-α, monocyte chemoattractant protein-1 (MCP-1), and NLR family pyrin domain containing 3 (Fig. 2J), and interleukin-6 (IL-6) secretion were increased in Pex5 knockdown adipocytes (Fig. 2K).

H_2O_2 suppresses peroxisome biogenesis in 3T3-L1 adipocytes

As oxidative stress plays a role in the adipocyte injury (13), we determined whether it also affects peroxisomal biogenesis. H_2O_2 decreased Pex5, Pex11α, Pex14, catalase, and Acox1 mRNA levels in a dose-dependent manner (Fig. 3A), which were significantly inhibited by a well-known antioxidant *N*-acetyl-cysteine (NAC) (Fig. 3B, C). In addition to ROS, inflammatory cytokines contribute to downregulation of peroxisomal genes (32). TNF-α, one of major inflammatory cytokines, significantly decreased Pex5, Abcd3, and

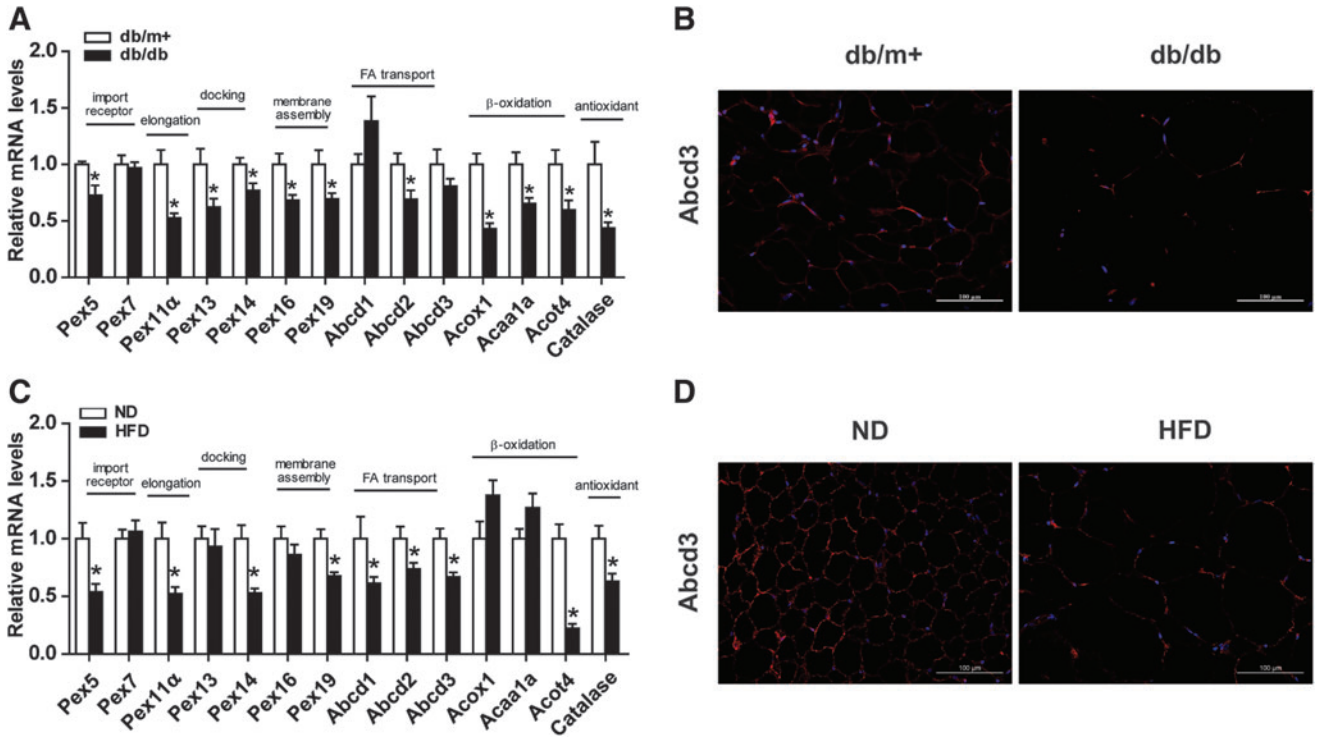

FIG. 1. WAT of obese mice exhibits decreased peroxisomal abundance. (A) Relative mRNA levels of genes related to peroxisome biogenesis and function were measured in WAT of db/m$^+$, db/db, as well as **(C)** ND and HFD-fed mice. **(B)** Immunostaining of Abcd3 (*red*) and DAPI nuclear counterstains (*blue*) in WAT of 20-week-old db/db and **(D)** HFD-fed mice. Original magnification: 200×; scale bar: 100 μm. **(A–D)** Values are mean ± SE of 5–7 mice. *$p < 0.05$ *versus* db/m$^+$ mice or ND mice. DAPI, 4′,6-diamidino-2-phenylindole; HFD, high-fat diet; ND, normal diet; SE, standard error; WAT, white adipose tissue. Color images are available online.

catalase protein expression, which indirectly represent reduction of peroxisomal biogenesis and function (Fig. 3D, E).

HFD-fed CKO mice demonstrate an accelerated obesity and suppressed peroxisome biogenesis

Since catalase is a major peroxisomal antioxidant enzyme, we used CKO mice to replicate a condition of increased peroxisomal oxidative stress. Before HFD feeding, there was no significant difference in body weight across four experimental groups (Fig. 4A). Twelve-week-HFD feeding significantly increased wild-type (WT) and CKO mice's body weight as compared with those of respective controls (Fig. 4A). Subcutaneous and epididymal fat weights were particularly higher in HFD-fed CKO mice than HFD-fed WT mice (Fig. 4B–E). Histological hematoxylin and eosin (H&E) staining indicated that adipocytes were larger in WAT of HFD-fed CKO mice (Fig. 4F, G).

Dysregulated adipokine, inflammation, and oxidative stress have been well considered as major players in adipose tissue dysfunction (13, 38). F4/80 staining revealed that macrophage infiltration in WAT was increased in CKO mice compared with WT mice under HFD feeding (Fig. 4H). Accordingly, adiponectin and IL-10 mRNA levels were downregulated, whereas MCP-1, F4/80, and CD11c mRNA levels were increased in WAT of HFD-fed CKO mice (Fig. 4I). Lipid peroxides (LPOs), detected in both plasma and WAT, were significantly higher in HFD-fed CKO mice than in WT mice (Fig. 4J, K). Other oxidative stress markers, that is, 4-hydroxynonenal (4-HNE) and 8-hydroxydeoxyguanosine (8-oxo-dG), were also significantly increased in WAT of HFD-fed CKO mice (Fig. 4L–N).

Importantly, WAT of HFD-fed CKO mice demonstrated decreased peroxisomal protein expression, that is, Pex5, Pex14, Pex16, Abcd3, and Acox1 (Fig. 4O, P). A similar trend was also observed in the transcript levels of Pex5, Pex14, Abcd2, and Acot4 (Fig. 4Q). However, these pathological changes and decreased peroxisomal protein expression were not observed in ND-fed CKO mice (Supplementary Fig. S3). These results suggest that catalase deficiency exacerbates oxidative stress in WAT under high-fat-induced metabolic stress, which is associated with suppressed peroxisomal biogenesis and accelerated obesity. Thus, increasing peroxisomal biogenesis can be a beneficial strategy in ameliorating HFD-induced adipocyte injury.

Fenofibrate rescues peroxisomal dysfunction in WAT and ameliorates adipocyte injuries in HFD-induced obese mice

To dissect beneficial effects of restoring peroxisomal function in WAT, HFD-fed WT mice were treated with a PPARα agonist (fenofibrate), a classical peroxisome proliferator, which may induce peroxisomal biogenesis in WAT (27, 40). Protein expression of key regulators in peroxisomal biogenesis, that is, Pex5, Pex14, and Pex16, was significantly decreased in WAT of HFD-fed WT mice. Abcd3 staining further confirmed that peroxisome was less abundant in WAT of HFD-fed WT mice than in ND-fed WT mice. HFD-fed WT mice treated with fenofibrate demonstrated significant restorations of peroxisomal biogenesis and abundance (Fig. 5A–D).

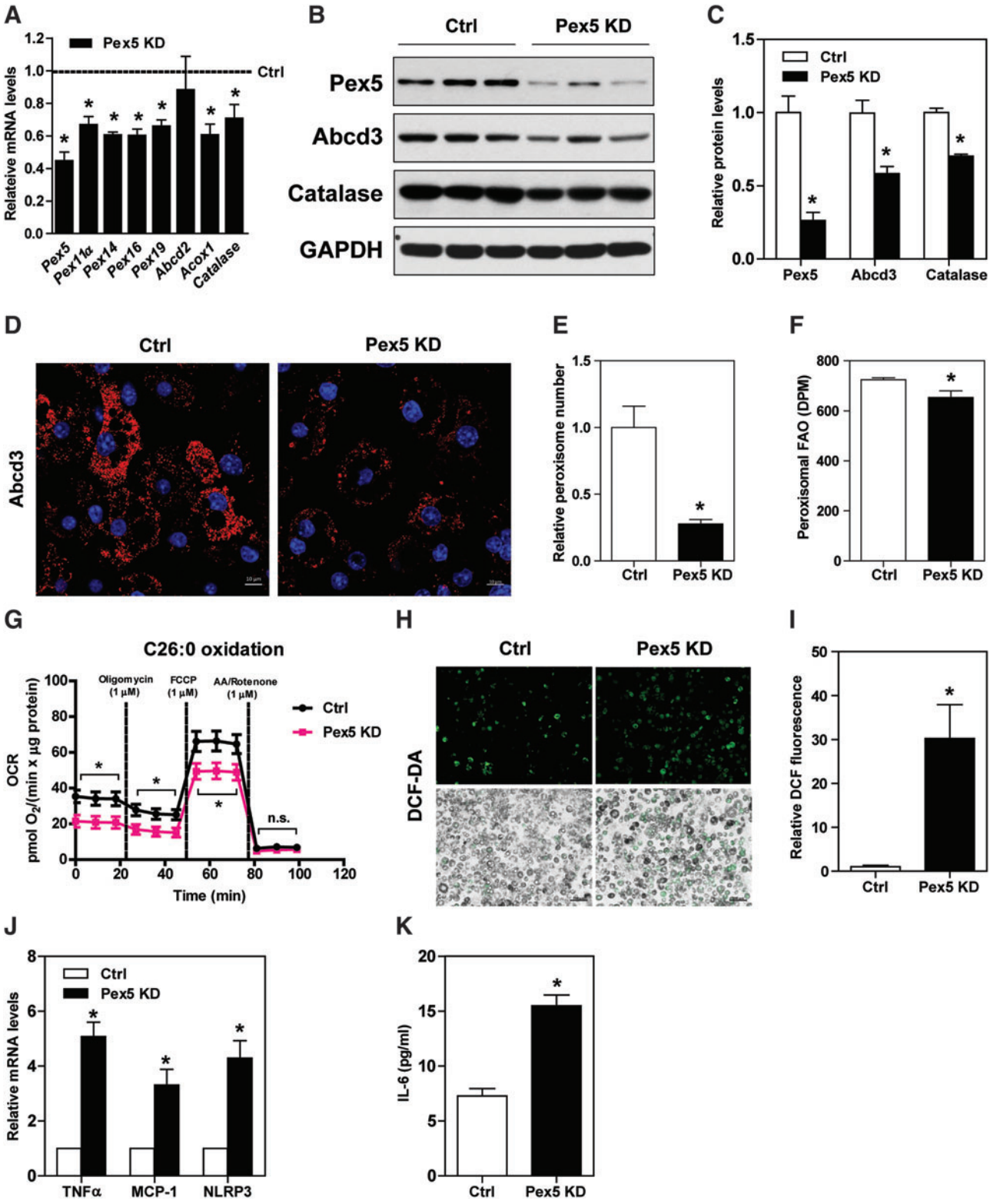

FIG. 2. Pex5 knockdown exacerbates ROS and inflammation in 3T3-L1 adipocytes. **(A–C)** 3T3-L1 adipocytes were transfected with Pex5 siRNAs for 72 h. Reductions of Pex5 mRNA and protein expressions were verified. Gene and protein expressions related to peroxisome biogenesis and function were measured. Expression levels of indicated proteins were quantified by densitometry and normalized with GAPDH. **(D)** Immunostaining and **(E)** fluorescence-intensity quantification of Abcd3 in control and Pex5 knockdown adipocytes. Original magnification: 630×; scale bar: 10 μm. **(F)** Measurement of adipose tissue peroxisomal FAO and **(G)** OCR in the presence of 10 μM hexacosanoic acid (C26:0). **(H)** Cellular ROS was detected with DCF-DA and **(I)** staining intensity was quantified. Original magnification: 100×; scale bar: 100 μm. **(J)** Relative mRNA levels of inflammatory cytokines are shown. **(K)** Secreted IL-6 in cell culture supernatant was measured by enzyme-linked immunosorbent assay. **(A–K)** Values are mean ± SE of 3–4 experiments. *$p < 0.05$ *versus* control. DCF-DA, 2′,7′–dichlorofluorescein diacetate; DPM, disintegrations per minute; FAO, fatty acid oxidation; OCR, oxygen consumption rate; Pex, peroxisomal biogenesis factor; ROS, reactive oxygen species. Color images are available online.

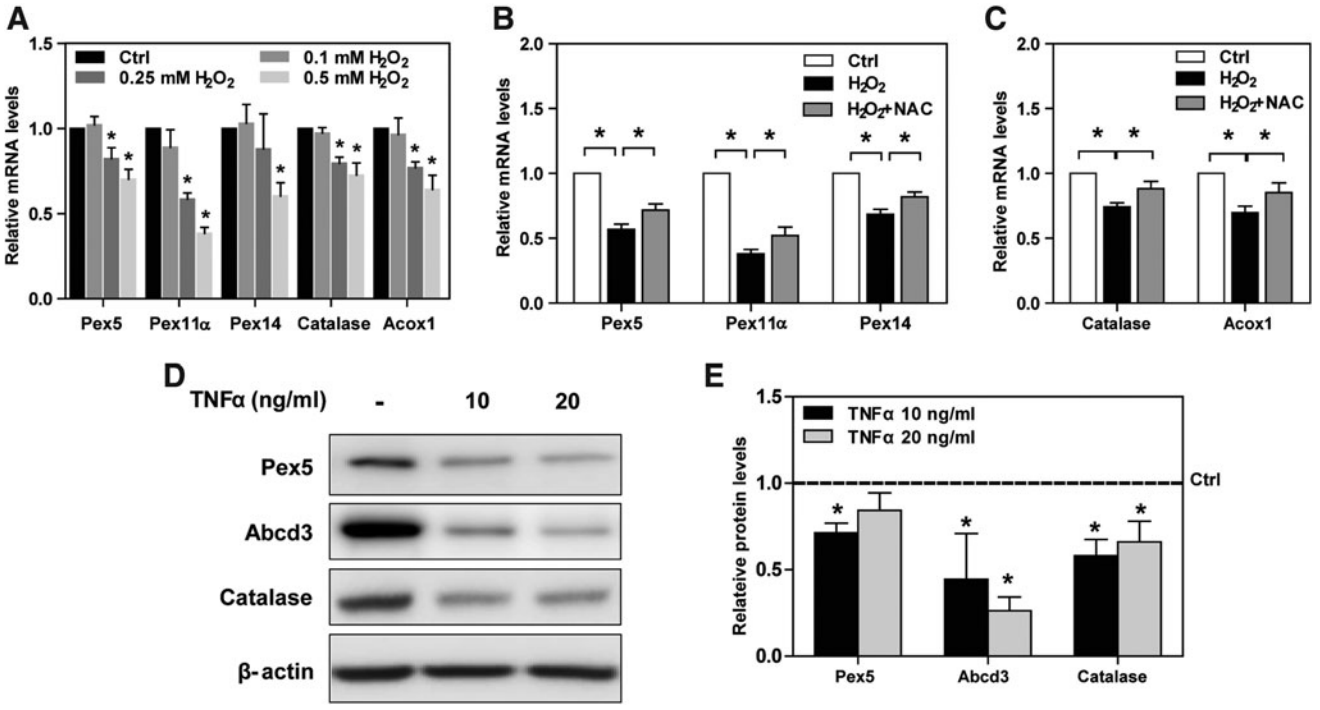

FIG. 3. H_2O_2 induces downregulation of peroxisome biogenesis in 3T3-L1 adipocytes. (A) Mature 3T3-L1 adipocytes were treated with three different concentrations of H_2O_2 (0.1, 0.25, and 0.5 m*M*). Relative mRNA levels of peroxisomal genes were examined by quantitative polymerase chain reaction. **(B, C)** After a pretreatment with 10 m*M* NAC, mature 3T3-L1 adipocytes were treated with 0.5 m*M* H_2O_2 for 6 h. Relative mRNA levels of peroxisomal genes were measured. **(D)** Mature 3T3-L1 adipocytes were treated with either 10 or 20 ng/mL TNF-α for 24 h. Pex5, Abcd3, and catalase protein expression was analyzed with Western blotting. **(E)** Expression levels of indicated proteins were quantified by densitometry and normalized with β-actin. **(A–E)** Values are mean ± SE of 3–4 experiments. $*p < 0.05$ *versus* control. H_2O_2, hydrogen peroxide; NAC, *N*-acetyl cysteine; TNF-α, tumor necrosis factor-α.

Compared with ND-fed WT mice, HFD-fed WT mice exhibited decreased peroxisomal FAO in WAT, which were significantly attenuated by fenofibrate treatment (Fig. 5E). Protein expression of Abcd3, Acox1, and catalase was also reduced in HFD-fed WT mice, which was significantly increased in response to fenofibrate treatment (Fig. 5F, G). However, these beneficial effects of fenofibrate were absent in WAT of ND-fed mice (Supplementary Fig. S4).

As fenofibrate maintains peroxisomal fitness in WAT, we investigated whether fenofibrate ameliorates adipocytes injury. F4/80 immunostaining in WAT of HFD-fed WT mice confirmed macrophage infiltration and crown-like structure around necrotic adipocytes, which were significantly alleviated in response to fenofibrate (Fig. 6A, B). Moreover, WAT of HFD-fed WT mice exhibited a decrease in adiponectin mRNA level, which was restored by fenofibrate treatment. Proinflammatory mediators, such as MCP-1, F4/80, and CD11c (a representative marker of M1 macrophage), were increased in WAT of HFD-fed WT mice, which were significantly decreased in response to fenofibrate (Fig. 6C). Increased oxidative stress, indicated by plasma LPO, WAT LPO, and 8-oxo-dG, in WAT of HFD-fed WT mice was also significantly decreased by fenofibrate (Fig. 6D–F).

In addition, HFD-fed WT mice treated with fenofibrate confirmed weight loss, which was mainly attributed to decreases in subcutaneous and epididymal fat (Supplementary Fig. S5). Fenofibrate treatment also showed an improved insulin sensitivity as evaluated by homeostatic model assessment for insulin resistance index, intraperitoneal glucose tolerance test (IPGTT), and intraperitoneal insulin tolerance test (IPITT) (Supplementary Fig. S6).

Pharmacological effects of fenofibrate were interestingly observed in obese HFD-fed CKO mice. HFD-fed CKO mice treated with fenofibrate demonstrated increases in peroxisomal biogenesis-related genes, glucose tolerance, and insulin sensitivity, along with decreases in body weight, fat weight, adipocyte size, plasma and WAT LPO, as well as F4/80 and nitrotyrosine-positive staining area in WAT (Supplementary Fig. S7).

Fenofibrate-induced peroxisomal biogenesis and function depend on PPARα

PPARα plays a role in regulating hepatic peroxisomal proliferation (9, 21). Fenofibrate's mode of action, however, is not restricted to PPARα agonism. Therefore, we examined whether fenofibrate-induced peroxisomal biogenesis depended on PPARα activation. Fenofibrate did not decrease either the adiposity (Supplementary Fig. S8A–E) or oxidative stress, indicated by 8-oxo-dG staining (Supplementary Fig. S8F), in WAT of HFD-fed PPARα KO mice. Beneficial effects of fenofibrate on peroxisomal biogenesis-related proteins, that is, Pex5, Pex11α, and Pex16, peroxisomal abundance indicated by Abcd3 immunostaining, and peroxisomal FAO were absent in WAT of HFD-fed PPARα KO mice (Supplementary Fig. S9).

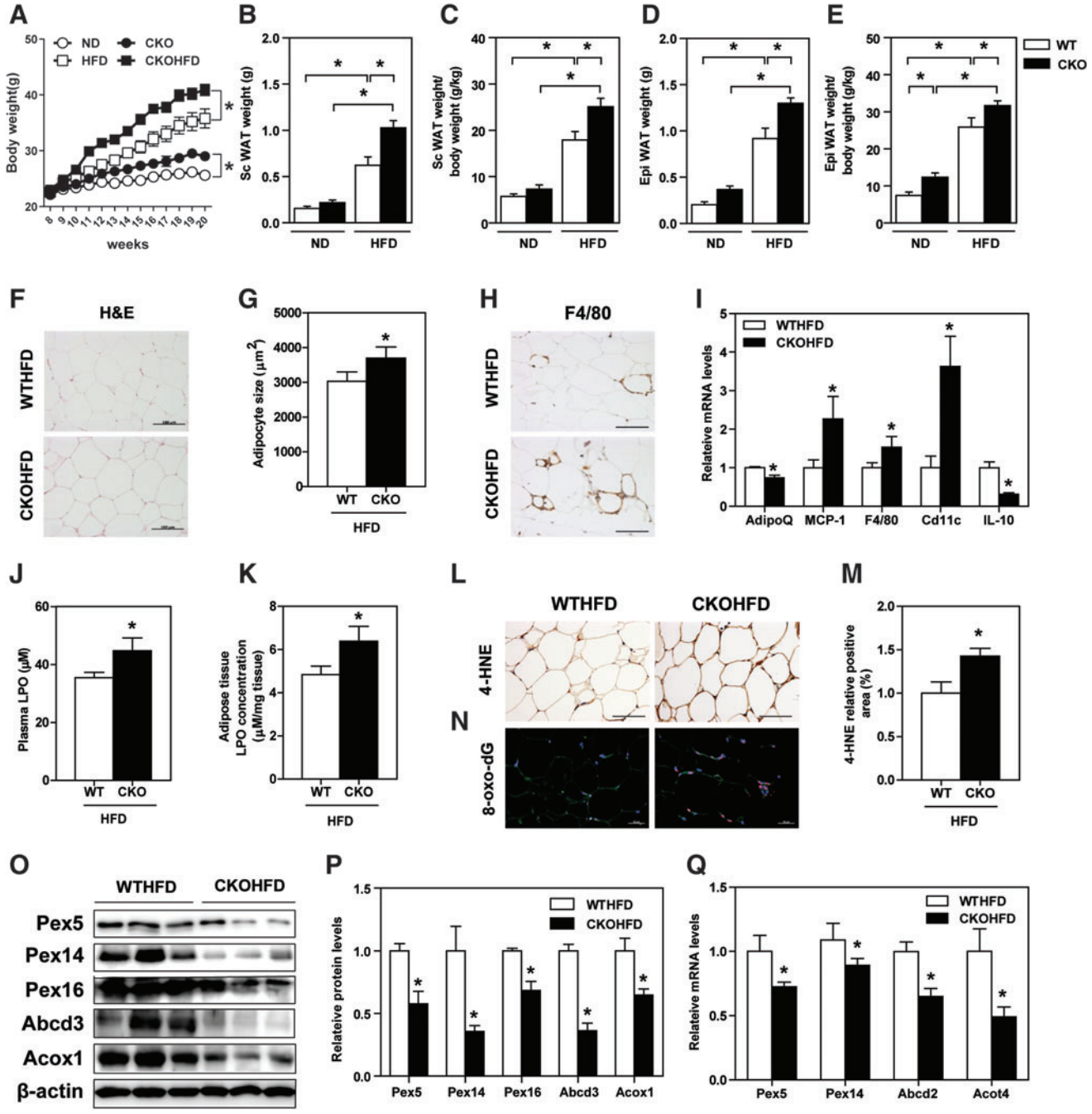

FIG. 4. HFD-fed CKO mice demonstrate accelerated obesity and suppressed WAT peroxisome biogenesis. (**A**) Body weight of HFD-fed WT and CKO mice was measured every week. (**B**–**E**) Subcutaneous and epididymal WAT weight, before and after corrected by body weight. (**F**) H&E staining, (**G**) quantification of adipocyte size, and (**H**) F4/80 immunostaining of WAT are shown. (**I**) mRNA levels of adiponectin and inflammation-related genes were analyzed. (**J**) Plasma and (**K**) WAT LPO levels were measured. (**L**) 4-HNE immunostaining of WAT and (**M**) quantification of positive staining area are shown. (**N**) 8-oxo-dG immunostaining analysis of WAT. (**O**–**Q**) Protein and mRNA expressions of peroxisomal proteins are shown. Expression levels of indicated proteins were quantified by densitometry and normalized with β-actin. Figures' original magnification: 200×; scale bar: 100 μm (**F**, **H**, and **L**), 50 μm (**N**). (**A**–**Q**) Values represent means ± SE of seven mice per group. *$p < 0.05$ *versus* WT HFD mice. 4-HNE, 4-hydroxynonenal; 8-oxo-dG, 8--hydroxydeoxyguanosine; CKO, catalase knock out; H&E, hematoxylin and eosin; LPO, lipid peroxides; WT, wild-type. Color images are available online.

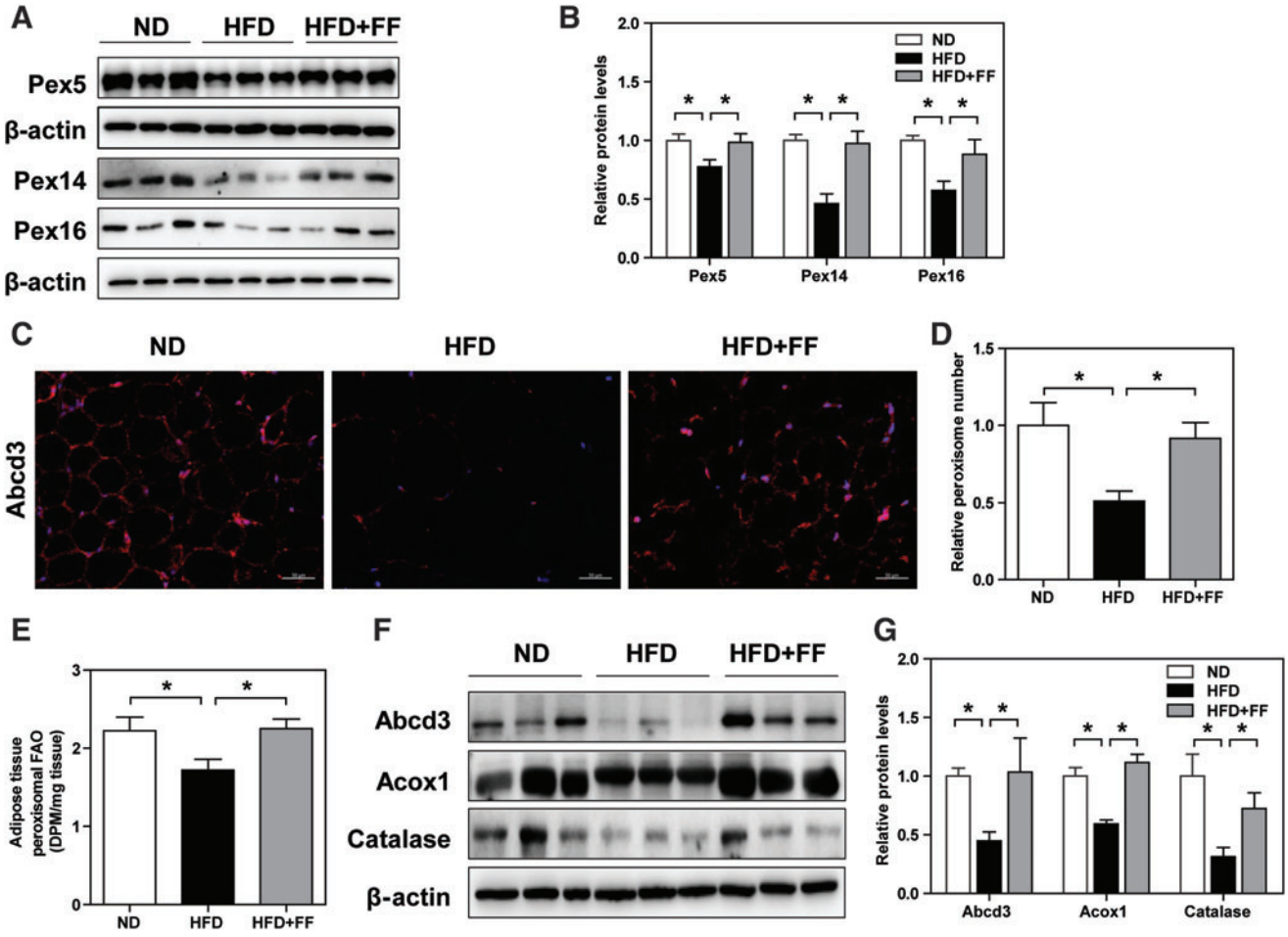

FIG. 5. Fenofibrate attenuates peroxisomal dysfunction in WAT of HFD-fed WT mice. (A, B) Western blot analysis of Pex5, Pex14, and Pex16 protein expression in WAT. **(C)** Immunostaining and **(D)** fluorescence-intensity quantification of Abcd3. Original magnification: 200×; scale bar: 50 μm. **(E)** Measurement of peroxisomal FAO in WAT. **(F, G)** Western blot analysis of Abcd3, Acox1, and catalase protein expression in WAT. Expression levels of indicated proteins were quantified by densitometry and normalized with β-actin. **(A–G)** Values represent mean ± SE of seven mice. *$p < 0.05$. Color images are available online.

Discussion

This study advanced our understanding on the role of peroxisome in adipose tissue dysfunction associated with obesity. We found that peroxisomal genes were significantly downregulated in WAT of diabetic obese db/db and HFD-induced obese mice. A similar finding has been reported in the liver of mice with nonalcoholic fatty liver disease (33), which is also a feature of obesity-associated metabolic syndrome. Interestingly, our preliminary study (data not shown) and a Gene Expression Omnibus database (GSE94753) analysis (25) (Supplementary Fig. S1H) revealed that WATs of obese human had lower peroxisomal genes than those of healthy lean individuals. In fact, a couple of independent clinical studies demonstrated pathological changes associated with peroxisomal dysfunction in patients with metabolic syndrome, such as a high VLCFA concentration in the whole blood (26) and low level of plasmalogens, which are a subtype of ether-linked phospholipids synthesized in peroxisome (8). This evidence suggests that peroxisome dysfunction plays an important role in mediating the pathogenesis of metabolic syndrome as well as obesity.

We have, then, investigated the key event that is responsible for WAT peroxisomal gene downregulations during obesity. As H_2O_2 in WAT was prominently increased in obese mice and suggested to be an important driver of metabolic syndrome (13), we examined the effect of oxidative stress on peroxisomal fitness. H_2O_2 significantly decreased peroxisomal genes in differentiated 3T3-L1 adipocytes, which were significantly inhibited by NAC. However, further studies are necessary to investigate the effect of either other antioxidants or catalase overexpression in oxidative stress-induced peroxisomal dysfunction. It should be noticed that ROS may interact with proteins and cause protein oxidative modifications. In mouse embryo fibroblast cells, H_2O_2 modified catalase activation based on its concentration (5, 6). Therefore, it remains interesting to investigate whether peroxisomal proteins, including catalase, are modified under metabolic stress-induced oxidative stress in adipose tissues.

Since ROS are intimately associated with inflammatory response (3), we examined the effect of inflammation on peroxisome. TNF-α decreased peroxisomal proteins in 3T3-L1 adipocytes. Similar to our result, Pex13 expression in lung

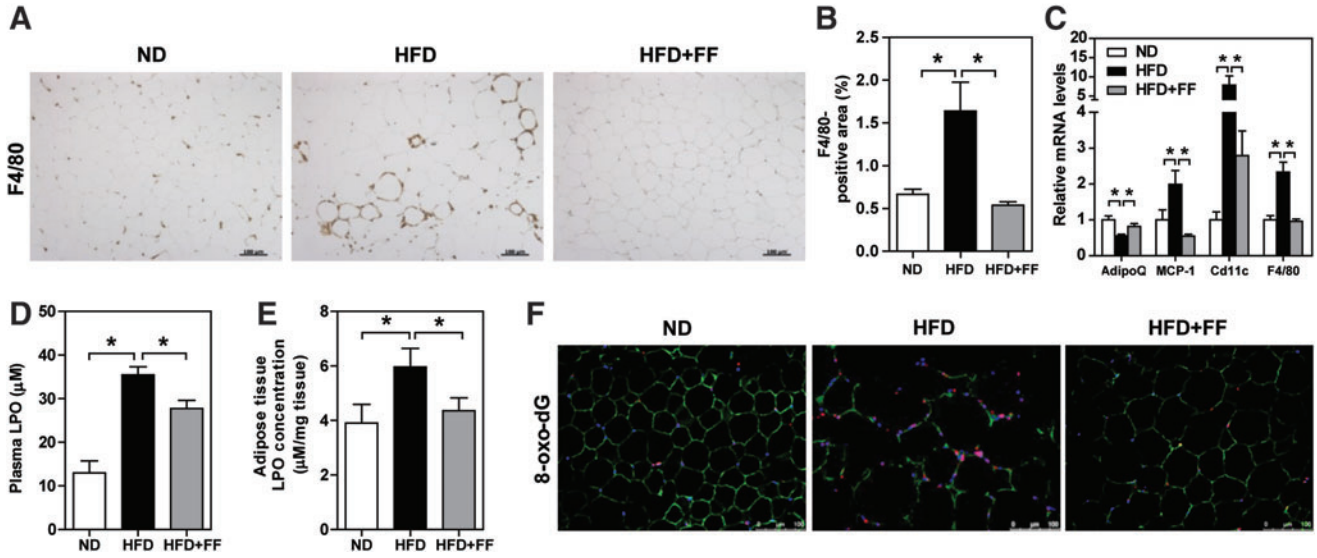

FIG. 6. Fenofibrate ameliorates adipocytes injury in WAT of HFD-fed WT mice. **(A)** F4/80 immunostaining and **(B)** quantitative analysis of positive staining area. Original magnification: 100×; scale bar: 100 μm. **(C)** Relative mRNA levels of adipokine and proinflammatory cytokines in WAT were analyzed. **(D)** Plasma and **(E)** WAT LPO levels were measured. **(F)** Coimmunostaining of 8-oxo-dG, perilipin, and DAPI in WAT. Original magnification: 200×; scale bar: 100 μm. **(A–F)** Values represent mean ± SE of seven mice. $^*p < 0.05$. Color images are available online.

fibroblast was decreased in response to TNF-α stimulation (32). On the contrary, Pex5 knockdown in mature adipocytes increased cellular ROS and inflammatory cytokines, and suppressed peroxisomal abundance and FAO. Consistent with our results, Pex13 (32) or Pex11β (1) deficiency led to increased oxidative stress in lung fibroblast or neurons, respectively. Altogether, we showed a positive feedback loop of oxidative stress/inflammation and peroxisomal dysfunction, which exaggerates adipose tissue dysfunction.

Considering that various peroxins are involved in peroxisomal biogenesis and function, other Pex gene knockdowns remain important to thoroughly understand the relation between peroxisomal oxidative stress and biogenesis in WAT. To clearly show the role of peroxisomal oxidative stress, it is also needed to perform spatiotemporal measurement of peroxisomal H_2O_2 by using peroxisomal-targeted H_2O_2 sensitive fluorescent probe (HyPer) (35).

The results from 3T3-L1 adipocytes culture were confirmed in the HFD-induced obese mice. Metabolic stress-induced obesity and exacerbated inflammation and oxidative stress in WAT were associated with decreased peroxisomal FAO as well as expression of proteins related to peroxisomal biogenesis and function. In this study, we used a common diet-induced obesity model, that is, HFD, which is mainly rich in oleic acid, linoleic acid, and palmitic acid. Further studies utilizing diet enriched with phytol, a branched-chain fatty acid mainly metabolized in the peroxisome, are needed to confirm the role of peroxisome in adipose tissues.

Similar to our previous study in diabetic kidney (20), CKO mice decreased peroxisomal gene expressions in adipocytes. CKO mice with dysfunctional peroxisomes and aggravated oxidative stress demonstrated accelerated HFD-induced obesity, WAT inflammation, and suppression of adiponectin, compared with WT mice. Since catalase in nonadipocyte tissues may also contribute to metabolic dysregulation, a further study with adipose tissue-specific catalase-deficient mice is important.

As observed in other studies (11, 23, 41), adipocyte hypertrophy and insulin resistance in HFD-fed WT mice were effectively prevented by fenofibrate. Peroxisomal β-oxidation was significantly recovered in WAT of HFD-fed WT mice with fenofibrate treatment. Improvement of peroxisomal biogenesis and function accentuated fenofibrate's therapeutic effect in ameliorating fasting-refeeding-induced liver damage (27) and deoxycorticosterone acetate-salt-induced kidney injury (40).

The effect of fenofibrate in restoring peroxisomal fitness could be attributed to PPARα activation. PPARα agonist, such as WY-14643 and clofibrate, has been shown to increase peroxisomal abundance and genes related to peroxisomal FAO in the liver of WT mice, but not in mice with nonfunctional, mutant PPARα (28). This notion was confirmed by our results, showing that fenofibrate's therapeutic effects were absent in PPARα KO mice.

Although we cannot exclude the plausibility of metabolic improvement from fenofibrate binding to PPARα in other nonadipose tissue, several *in vitro* studies have suggested that fenofibrate can directly attenuate adipose tissue inflammation (17, 39). A further study with adipose tissue-specific PPARα KO mice is important to elucidate the role of adipose tissue PPARα in metabolic profile improvement by fenofibrate. Meanwhile, our preliminary results (data not shown) and previous studies have suggested that PPARδ and PPARγ are also expressed and contribute in maintaining peroxisomal biogenesis and function in the WAT (19, 36). All these PPAR subtypes apparently coordinate both peroxisomal biogenesis and integrative lipid metabolism. In this study, we showed that maintaining peroxisomal fitness, partially by activating PPARα through fenofibrate treatment, significantly contributed to attenuate HFD-induced adipocytes injury.

In summary, we have shown that decreased peroxisomal biogenesis and function are associated with obesity progression. A positive feedback loop of downregulated

peroxisomal biogenesis and increased ROS/inflammatory mediators may be responsible for exacerbating adipose dysfunction (Fig. 7). The temporal aspect of ROS, inflammation, and peroxisomal downregulation has not been clearly shown due to lack of sensitive methods to detect each parameter. However, activation of peroxisomal biogenesis, partially through PPARα activation, enhances peroxisomal FAO and attenuates adiposity. Therefore, a further investigation on peroxisomal biogenesis remains interesting to understand the pathogenesis of obesity more meticulously and to establish a more effective therapeutic strategy in obesity as well as other metabolic disorders.

Materials and Methods

Chemicals and reagents

All chemicals were obtained from Sigma-Aldrich (St. Louis, MO) unless otherwise stated.

Animals

Whole-body CKO (18) and PPARα KO (2) mice with C57BL/6J background were generated as described previously. Eight-week-old male WT, CKO, and PPARα KO mice were housed in a temperature-controlled room on a 12-h light–dark cycle, 3–4 mice were conditioned in each cage. Mice were fed with either ND (10% fat, saturated fat 22.7% of fat, monounsaturated fat 29.9% of fat, polyunsaturated fat 47.4% of fat, and cholesterol 51.6 mg/kg; Research Diets, Product No. D12450) or HFD (60% fat, saturated fat 32% of fat, monounsaturated fat 35.9% of fat, polyunsaturated fat 32% of fat, and cholesterol 279.6 mg/kg; Research Diets, Product No. D12492), along with tap water *ad libitum* for 12 weeks.

Fenofibrate (Sigma-Aldrich; Product No. F6020) 50 mg/kg/day was administered orally along with the initiation of HFD. The control ND and HFD groups were administered an equal volume of 0.5% carboxymethyl cellulose by oral gavage. C57BLKS/J-db/db and age-matched control C57BLKS/J-m+/db mice (Japan SLC, Inc., Hamamatsu, Japan) were housed under the same condition as other experimental animals; these mice were fed with ND and sacrificed at 20 weeks of age. All animal studies were approved by the Institutional Animal Care and Use Committee of Ewha Womans University (No. 15-062).

Measurement of blood parameters

Blood glucose was measured with OneTouch Ultra glucometer (LifeScan, Milpitas, CA). To collect plasma samples, blood was centrifuged at 4°C, 3000 rpm for 15 min. Fasting plasma insulin level was measured with a commercial ELISA kit (EMD Millipore Corporation, Billerica, MA; Product No. EZRMI-13K) according to the manufacturer's protocol.

Glucose tolerance test and insulin tolerance test

IPGTT was performed by injecting 1.0 g glucose/kg body weight after 16-h fasting. One week later, IPITT was conducted by injecting 0.75 U/kg body weight Humulin R (Eli Lilly, Indianapolis, IN) after 6-h food deprivation. Blood glucose was measured by OneTouch Ultra glucometer at

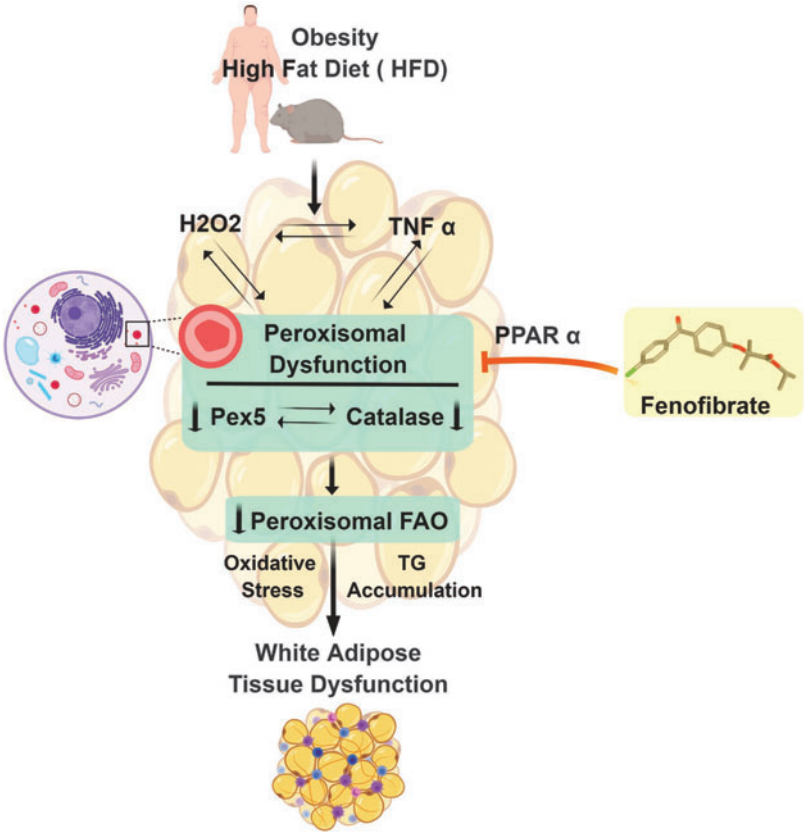

FIG. 7. Schematic illustration. A positive feedback loop of oxidative stress/inflammation and peroxisome downregulation exacerbates adipocyte dysfunction and obesity progression. Fenofibrate, a peroxisome proliferator, significantly attenuates adipocyte dysfunction in obese HFD-fed mice. Color images are available online.

0, 15, 30, 60, 90, and 120 min after glucose or insulin administration.

3T3-L1 cell culture and differentiation

Murine 3T3-L1 preadipocytes were purchased from American Type Culture Collection (Manassas, VA), and maintained in Dulbecco's Modified Eagle Medium (DMEM) high glucose (Gibco, Grand Island, NY) supplemented with 10% bovine calf serum (Gibco), at 37°C in humidified 5% CO_2 in the air. Two days postconfluence (day 0), cells were incubated in DMEM containing 10% fetal bovine serum (FBS; Gibco), 1 μM dexamethasone (Sigma-Aldrich; Product No. D-4902), 5 μg/mL insulin (Sigma-Aldrich; Product No. I0516), and 0.5 m*M* isobutylmethylxanthione (Sigma-Aldrich; Product No. I-7018). On day 2, medium was replaced with 10% FBS DMEM supplemented with 5 μg/mL insulin. Starting on day 4, the medium was replaced with fresh 10% FBS DMEM every 2 days. Mature adipocytes were used for experiment.

Pex5 siRNA transfection in mature adipocytes

In brief, Pex5 siRNA were incubated with TransIT-X2 reagent (Mirus Bio, WI; Product No. MIR6000) in basal media with serum and antibiotics, and allowed to form a complex within 30 min at room temperature. The complex was then added to cell suspension in each well. Silencing efficiency with different doses, that is, 20, 50, 70, and 100 n*M*, was confirmed by analyzing gene and protein expression.

Measurement of cellular C26:0-oxidation

Differentiated 3T3-L1 cells were plated in Cell-Tak™ coated XF24 polystyrene cell culture microplates (Seahorse Bioscience, Agilent; Product No. 100777-004) at a density of 10,000 cells per well. After 24 h, cells were washed and preincubated for 30 min in XF assay medium at 37°C. Oxygen consumption rate was subsequently measured every 12 min using an XF24 extracellular flux analyzer (Seahorse Bioscience, Agilent). For measurement of cellular hexacosanoic acid (C26:0) oxidation capacity, control and siPex5 adipocytes were incubated with 10 μM C26:0/ethanol-containing assay medium 45 min before and during the measurement. Oxygen consumption was normalized to protein concentration (pmol/min × μg protein).

Measurement of peroxisomal FAO

FAO was measured as previously described (22). Adipose tissue homogenates (50 μL) were added to reaction buffer containing 0.2 m*M* palmitate (^{14}C-palmitate at 1.25 μCi/mL; NEN Life Science, Boston, MA; Product No. NEC075H250UC). After 2 h incubation at 30°C, the reaction was quenched by the addition of 50 μL of 4 N sulfuric acid. CO_2 produced during 2 h incubation was trapped with 200 μL of 1 N sodium hydroxide. The trapped $^{14}CO_2$ was then measured by liquid scintillation counting, and the rate of FAO was normalized to protein content of each sample. Peroxisomal FAO was measured in the presence of 100 μM antimycin A and 12.5 μM rotenone, which are inhibitors of mitochondrial oxidation.

Measurement of cellular ROS

For measuring intracellular ROS, differentiated 3T3-L1 adipocytes were incubated for 30 min at 37°C with 10 μM 5-(and 6)-chloromethyl-DCF-DA (Invitrogen, Eugene, OR; Product No. C6827). After twice washing with prewarmed phosphate-buffered saline, the fluorescence intensity was detected by ZEISS Apotome.2 (Carl Zeiss, Thornwood, NY).

Measurement of IL-6 cell culture supernatant

Mature adipocytes were transfected with Pex5 or control siRNA, and 72 h after transfection the supernatants were collected and levels of secreted cytokines were analyzed using mouse IL-6 Quantikine ELISA kit (R&D, Minneapolis, MN; Product No. M6000B), according to the manufacturer's instructions.

Measurement of LPO

Plasma level of LPO was measured as thiobarbituric acid reactive substances (16). In brief, plasma aliquots were mixed with 8% sodium dodecyl sulfate (SDS) and a mixture containing 0.8% 2-thiobarbituric acid and 20% acetic acid. This solution was kept at 95°C for 60 min. After stopping the reaction by cooling it down, the mixture was centrifuged at 4000 rpm for 5 min to precipitate interfering particulate materials. The amount of LPO in the plasma was measured by spectrofluorometry. Meanwhile, LPO level in WAT was measured using LPO assay kit (Cayman Chemical, Ann Arbor, MI; Product No. 705003) according to the manufacturer's protocol.

Histology and immunohistochemical staining

Adipose tissues were fixed with 4% formalin, dehydrated, and embedded in paraffin for histological studies. Five-micrometer epididymal fat sections from mice were stained with H&E, and adipocyte size was quantified as described previously (34). Immunohistochemical staining was performed using immunoperoxidase procedures from a commercially available kit (Dako, Glostrup, Denmark). The adipose tissue sections were deparaffinized, and endogenous peroxidase was blocked with peroxidase solution (Dako; Product No. S2023) for 30 min. Then, sections were incubated with serum-free blocking solution (Dako; Product No. X0909) before overnight incubation with the primary antibodies; that is, anti-F4/80 (1:200; Santa Cruz Biotechnology, Inc., Santa Cruz, CA; Product No. sc-71088), antinitrotyrosine (1:200, Product No. sc-32758; Santa Cruz), or anti-4-HNE (1:200, Product No. MHN-100P; JaICA, Fukuroi, Japan) at 4°C. Sections were then incubated with secondary antibodies and exposed to 3,3′-diaminobenzidine (Dako; Product No. K3468) for 1 min. Images were captured with a Zeiss microscope (Carl Zeiss).

Immunofluorescence staining

After deparaffinization and rehydration, tissue sections were incubated with retrieval solution and heated in a microwave to recover antigenicity. Nonspecific binding was blocked with serum-free blocking solution for 30 min at room temperature. Adipose tissue sections were then incubated with anti-8-oxo-dG (1:200, Product No. 4353-MC-050; Trevigen, Gaithersburg, MD) or anti-Abcd3 (1:200, Product

No. ab85550; Abcam, Cambridge, MA) overnight at 4°C. Tissue sections were incubated for 1 h with Alexa 488-conjugated goat antimouse (1:1000, Product No. A11018; Invitrogen) or Alexa 568-conjugated goat antirabbit (1:1000, Product No. A11070; Invitrogen) antibody. Cell nuclei were detected with 4′,6-diamidino-2-phenylindole (1:1000, Product No. 62248; Thermo Fisher Scientific, Waltham, MA). Images were captured by ZEISS Apotome.2 (Carl Zeiss). The number of peroxisomes per cell was quantified by counting the number of Abcd3 positive organelles per cell, using ImageJ software.

Quantitative polymerase chain reaction

mRNA level was measured by real-time quantitative polymerase chain reaction using a SYBR Green PCR Master Mix kit (Applied Biosystems, Foster City, CA; Product No. 4367659) with a Stepone™ real-time PCR system (Applied Biosystems). Relative quantification of each gene was calculated after normalization to 18S rRNA. The primer sequences are listed in Supplementary Table S1.

Immunoblotting analysis

Adipose tissues were lysed and centrifuged at 13,000 rpm, 4°C for 15 min. Protein concentration was measured with Bradford methods (Bio-Rad Laboratories, Hercules, CA; Product No. 500-0006). Aliquots of tissue homogenates were mixed with sample buffer containing SDS and β-mercaptoethanol, and were heated at 95°C for 6 min. Samples were then applied to a SDS-polyacrylamide gel electrophoresis gel and separated by electrophoresis. Protein was transferred onto a polyvinylidene fluoride membrane (GE Healthcare BioSciences Co., Piscataway, NJ; Product No. BSP0161) in a transblot chamber with Tris buffer.

Membrane was subsequently blocked for 1 h at room temperature with 5% skim milk in TBS-Tween 20 buffer, followed by an overnight incubation at 4°C in a 1:1000 dilution of the indicated primary antibodies: anti-Abcd3 (1:1000, Product No. ab85550; Abcam), anti-Acox1 (1:1000, Product No. sc-98499; Santa Cruz), anticatalase (1:1000, Product No. sc-50508; Santa Cruz), anti-Pex5 (1:2000, Product No. sc-137135; Santa Cruz), anti-Pex11α (1:2000, Product No. ab104959; Abcam), anti-Pex14 (1:1000, Product No. sc-23197; Santa Cruz), anti-Pex16 (1:1000, Product No. 14816-1-AP; Proteintech Group, Rosemont, IL), anti-GAPDH (1:2000, Product No. 2118; Cell Signaling), and anti-β-actin (1:2000, Product No. A5326; Sigma-Aldrich).

Membrane was then washed and incubated with peroxidase-conjugated secondary antibody for 1 h at room temperature. After repeated washing, band was developed with an enhanced chemiluminescence detection reagent (GE Healthcare BioSciences Co.; Product No.RPN2235) according to the manufacturer's instructions. Positive immunoreactive bands were quantified with densitometer (LAS-3000; FUJIFILM Corporation, Tokyo, Japan), and were normalized with either GAPDH or β-actin for further statistical analysis. Uncropped images are shown in Supplementary Figure S10.

Statistical analysis

All results are expressed as means ± standard error. Using Statview 5.0 software, results were analyzed by one-way analysis of variance among multiple groups. The level of statistical significance was set at a p-value <0.05.

Acknowledgments

We thank Jung Hwa Lee for her technical assistance, and Ying Yu (Tianjin Medical University) for his critical reading and valuable advices. We are also immensely grateful to Ye-Shih Ho (Wayne State University) for providing CKO mice and Frank J. Gonzalez (National Institutes of Health/National Cancer Institute) for providing peroxisomal proliferator-activated receptor alpha KO mice.

Authors' Contributions

L.P., E.H.K, and H.H. were involved in conception and design of the experiment. L.P., D.D., and S.J. performed the experiments and analyzed the data. G.T.O. supplied peroxisomal proliferator-activated receptor alpha knockout mice. L.P. and D.D. contributed to drafting the article and revising it. H.H. made the final approval of the version to be published.

Author Disclosure Statement

No competing financial interests exist.

Funding Information

This work was financially supported by the grants from National Research Foundation of Korea (No. 2016R1A2B4 006575).

Supplementary Material

Supplementary Figure S1
Supplementary Figure S2
Supplementary Figure S3
Supplementary Figure S4
Supplementary Figure S5
Supplementary Figure S6
Supplementary Figure S7
Supplementary Figure S8
Supplementary Figure S9
Supplementary Figure S10
Supplementary Table S1

References

1. Ahlemeyer B, Gottwald M, and Baumgart-Vogt E. Deletion of a single allele of the Pex11beta gene is sufficient to cause oxidative stress, delayed differentiation and neuronal death in mouse brain. *Dis Model Mech* 5: 125–140, 2012.
2. Akiyama TE, Nicol CJ, Fievet C, Staels B, Ward JM, Auwerx J, Lee SS, Gonzalez FJ, and Peters JM. Peroxisome proliferator-activated receptor-alpha regulates lipid homeostasis, but is not associated with obesity: studies with congenic mouse lines. *J Biol Chem* 276: 39088–39093, 2001.
3. Alfadda AA and Sallam RM. Reactive oxygen species in health and disease. *J Biomed Biotechnol* 2012: 936486, 2012.
4. Baes M and Aubourg P. Peroxisomes, myelination, and axonal integrity in the CNS. *Neuroscientist* 15: 367–379, 2009.
5. Cao C, Leng Y, and Kufe D. Catalase activity is regulated by c-Abl and Arg in the oxidative stress response. *J Biol Chem* 278: 29667–29675, 2003.

6. Cao C, Leng Y, Li C, and Kufe D. Functional interaction between the c-Abl and Arg protein-tyrosine kinases in the oxidative stress response. *J Biol Chem* 278: 12961–12967, 2003.
7. Castro JP, Grune T, and Speckmann B. The two faces of reactive oxygen species (ROS) in adipocyte function and dysfunction. *Biol Chem* 397: 709–724, 2016.
8. Colas R, Sassolas A, Guichardant M, Cugnet-Anceau C, Moret M, Moulin P, Lagarde M, and Calzada C. LDL from obese patients with the metabolic syndrome show increased lipid peroxidation and activate platelets. *Diabetologia* 54: 2931–2940, 2011.
9. Dreyer C, Krey G, Keller H, Givel F, Helftenbein G, and Wahli W. Control of the peroxisomal beta-oxidation pathway by a novel family of nuclear hormone receptors. *Cell* 68: 879–887, 1992.
10. Elsner M, Gehrmann W, and Lenzen S. Peroxisome-generated hydrogen peroxide as important mediator of lipotoxicity in insulin-producing cells. *Diabetes* 60: 200–208, 2011.
11. Ferreira AV, Parreira GG, Green A, and Botion LM. Effects of fenofibrate on lipid metabolism in adipose tissue of rats. *Metabolism* 55: 731–735, 2006.
12. Fransen M, Nordgren M, Wang B, Apanasets O, and Van Veldhoven PP. Aging, age-related diseases and peroxisomes. *Subcell Biochem* 69: 45–65, 2013.
13. Furukawa S, Fujita T, Shimabukuro M, Iwaki M, Yamada Y, Nakajima Y, Nakayama O, Makishima M, Matsuda M, and Shimomura I. Increased oxidative stress in obesity and its impact on metabolic syndrome. *J Clin Invest* 114: 1752–1761, 2004.
14. Gould SJ and Valle D. Peroxisome biogenesis disorders: genetics and cell biology. *Trends Genet* 16: 340–345, 2000.
15. Grant RW and Dixit VD. Adipose tissue as an immunological organ. *Obesity (Silver Spring)* 23: 512–518, 2015.
16. Ha H, Yu MR, and Kim KH. Melatonin and taurine reduce early glomerulopathy in diabetic rats. *Free Radic Biol Med* 26: 944–950, 1999.
17. Hiuge A, Tenenbaum A, Maeda N, Benderly M, Kumada M, Fisman EZ, Tanne D, Matas Z, Hibuse T, Fujita K, Nishizawa H, Adler Y, Motro M, Kihara S, Shimomura I, Behar S, and Funahashi T. Effects of peroxisome proliferator-activated receptor ligands, bezafibrate and fenofibrate, on adiponectin level. *Arterioscler Thromb Vasc Biol* 27: 635–641, 2007.
18. Ho YS, Xiong Y, Ma W, Spector A, and Ho DS. Mice lacking catalase develop normally but show differential sensitivity to oxidant tissue injury. *J Biol Chem* 279: 32804–32812, 2004.
19. Hofer DC, Pessentheiner AR, Pelzmann HJ, Schlager S, Madreiter-Sokolowski CT, Kolb D, Eichmann TO, Rechberger G, Bilban M, Graier WF, Kratky D, and Bogner-Strauss JG. Critical role of the peroxisomal protein PEX16 in white adipocyte development and lipid homeostasis. *Biochim Biophys Acta* 1862: 358–368, 2017.
20. Hwang I, Lee J, Huh JY, Park J, Lee HB, Ho YS, and Ha H. Catalase deficiency accelerates diabetic renal injury through peroxisomal dysfunction. *Diabetes* 61: 728–738, 2012.
21. Issemann I and Green S. Activation of a member of the steroid hormone receptor superfamily by peroxisome proliferators. *Nature* 347: 645–650, 1990.
22. Jang JE, Park HS, Yoo HJ, Baek IJ, Yoon JE, Ko MS, Kim AR, Kim HS, Lee SE, Kim SW, Kim SJ, Leem J, Kang YM, Jung MK, Pack CG, Kim CJ, Sung CO, Lee IK, Park JY, Fernandez-Checa JC, Koh EH, and Lee KU. Protective role of endogenous plasmalogens against hepatic steatosis and steatohepatitis in mice. *Hepatology* 66: 416–431, 2017.
23. Jeong S and Yoon M. Fenofibrate inhibits adipocyte hypertrophy and insulin resistance by activating adipose PPARalpha in high fat diet-induced obese mice. *Exp Mol Med* 41: 397–405, 2009.
24. Kopelman P. Health risks associated with overweight and obesity. *Obes Rev* 8 Suppl 1: 13–17, 2007.
25. Kulyte A, Ehrlund A, Arner P, and Dahlman I. Global transcriptome profiling identifies KLF15 and SLC25A10 as modifiers of adipocytes insulin sensitivity in obese women. *PLoS One* 12: e0178485, 2017.
26. Kume A, Miyazaki T, Kitamura Y, Oshida K, Yanagisawab N, Takizawa H, Fujii K, Kiyanagi T, Sumiyoshi K, Ohmura H, Mokuno H, Shimada K, and Daida H. High levels of saturated very long-chain fatty acid (hexacosanoic acid; C26:0) in whole blood are associated with metabolic syndrome in Japanese men. *Diabetes Res Clin Pract* 80: 259–264, 2008.
27. Lee JN, Dutta RK, Kim SG, Lim JY, Kim SJ, Choe SK, Yoo KW, Song SR, Park DS, So HS, and Park R. Fenofibrate, a peroxisome proliferator-activated receptor alpha ligand, prevents abnormal liver function induced by a fasting-refeeding process. *Biochem Biophys Res Commun* 442: 22–27, 2013.
28. Lee SS, Pineau T, Drago J, Lee EJ, Owens JW, Kroetz DL, Fernandez-Salguero PM, Westphal H, and Gonzalez FJ. Targeted disruption of the alpha isoform of the peroxisome proliferator-activated receptor gene in mice results in abolishment of the pleiotropic effects of peroxisome proliferators. *Mol Cell Biol* 15: 3012–3022, 1995.
29. Lodhi IJ and Semenkovich CF. Peroxisomes: a nexus for lipid metabolism and cellular signaling. *Cell Metab* 19: 380–392, 2014.
30. Martens K, Bottelbergs A, Peeters A, Jacobs F, Espeel M, Carmeliet P, Van Veldhoven PP, and Baes M. Peroxisome deficient aP2-Pex5 knockout mice display impaired white adipocyte and muscle function concomitant with reduced adrenergic tone. *Mol Genet Metab* 107: 735–747, 2012.
31. Novikoff AB, Novikoff PM, Rosen OM, and Rubin CS. Organelle relationships in cultured 3T3-L1 preadipocytes. *J Cell Biol* 87: 180–196, 1980.
32. Oruqaj G, Karnati S, Vijayan V, Kotarkonda LK, Boateng E, Zhang W, Ruppert C, Gunther A, Shi W, and Baumgart-Vogt E. Compromised peroxisomes in idiopathic pulmonary fibrosis, a vicious cycle inducing a higher fibrotic response via TGF-beta signaling. *Proc Natl Acad Sci U S A* 112: E2048–E2057, 2015.
33. Park HS, Jang JE, Ko MS, Woo SH, Kim BJ, Kim HS, Park IS, Koh EH, and Lee KU. Statins increase mitochondrial and peroxisomal fatty acid oxidation in the liver and prevent non-alcoholic steatohepatitis in mice. *Diabetes Metab J* 40: 376–385, 2016.
34. Piao L, Jung I, Huh JY, Miyata T, and Ha H. A novel plasminogen activator inhibitor-1 inhibitor, TM5441, protects against high-fat diet-induced obesity and adipocyte injury in mice. *Br J Pharmacol* 173: 2622–2632, 2016.
35. Rhee SG, Chang TS, Jeong W, and Kang D. Methods for detection and measurement of hydrogen peroxide inside and outside of cells. *Mol Cells* 29: 539–549, 2010.
36. Roberts LD, Murray AJ, Menassa D, Ashmore T, Nicholls AW, and Griffin JL. The contrasting roles of PPARdelta and PPARgamma in regulating the metabolic switch between oxidation and storage of fats in white adipose tissue. *Genome Biol* 12: R75, 2011.

37. Van Gaal LF, Mertens IL, and De Block CE. Mechanisms linking obesity with cardiovascular disease. *Nature* 444: 875–880, 2006.
38. Vegiopoulos A, Rohm M, and Herzig S. Adipose tissue: between the extremes. *EMBO J* 36: 1999–2017, 2017.
39. Wang W, Lin Q, Lin R, Zhang J, Ren F, Ji M, and Li Y. PPARalpha agonist fenofibrate attenuates TNF-alpha-induced CD40 expression in 3T3-L1 adipocytes via the SIRT1-dependent signaling pathway. *Exp Cell Res* 319: 1523–1533, 2013.
40. Weng H, Ji X, Endo K, and Iwai N. Pex11a deficiency is associated with a reduced abundance of functional peroxisomes and aggravated renal interstitial lesions. *Hypertension* 64: 1054–1060, 2014.
41. Wu H, Wei L, Bao Y, Lu J, Huang P, Liu Y, Jia W, and Xiang K. Fenofibrate reduces serum retinol-binding protein-4 by suppressing its expression in adipose tissue. *Am J Physiol Endocrinol Metab* 296: E628–E634, 2009.

Address correspondence to:
Prof. Hunjoo Ha
Graduate School of Pharmaceutical Sciences
College of Pharmacy
Ewha Womans University
52, Ewhayeodae-gil, Seodaemun-gu
Seoul 03760
Republic of Korea

E-mail: hha@ewha.ac.kr

Date of first submission to ARS Central, July 19, 2018; date of final revised submission, September 16, 2019; date of acceptance, September 17, 2019.

Abbreviations Used

4-HNE = 4-hydroxynonenal
8-oxo-dG = 8-hydroxydeoxyguanosine
Abcd = ATP-binding cassette subfamily D
Acot4 = acyl-CoA thioesterase 4
Acox1 = acyl-CoA oxidase 1
CKO = catalase knock out
DAPI = 4′,6-diamidino-2-phenylindole
DCF-DA = 2′,7′–dichlorofluorescein diacetate
FAO = fatty acid oxidation
FBS = fetal bovine serum
H&E = hematoxylin and eosin
H_2O_2 = hydrogen peroxide
HFD = high-fat diet
IL = interleukin
IPGTT = intraperitoneal glucose tolerance test
IPITT = intraperitoneal insulin tolerance test
KO = knock out
LPO = lipid peroxides
MCP-1 = monocyte chemoattractant protein-1
NAC = *N*-acetyl-cysteine
ND = normal diet
Pex = peroxisomal biogenesis factor
PPARα = peroxisomal proliferator-activated receptor alpha
ROS = reactive oxygen species
SDS = sodium dodecyl sulfate
SE = standard error
TNF-α = tumor necrosis factor-α
VLCFA = very long-chain fatty acid
WAT = white adipose tissue
WT = wild-type